

## Angular anisotropy in the resonant Auger decay of $2p$ -photoexcited Mg

S. B. Whitfield,<sup>1</sup> U. Hergenhahn,<sup>1</sup> N. M. Kabachnik,<sup>1,\*</sup> B. Langer,<sup>1</sup> J. Tulkki,<sup>2</sup> and U. Becker<sup>1</sup>

<sup>1</sup>Fritz-Haber-Institut der Max-Planck-Gesellschaft, D-14195 Berlin, Germany

<sup>2</sup>Optoelectronics Laboratory, Helsinki University of Technology, SF-02150 Espoo, Finland

(Received 21 January 1994)

We have measured strongly negative  $\beta$  values of the  $3s$ -participator lines at the magnesium  $2p \rightarrow 4s$  and  $2p_{1/2} \rightarrow 3d$  excitations. Observed  $\beta$  values of the spectator lines following  $2p \rightarrow 4s$  excitation are not reproduced by the strict spectator model. Our multiconfiguration Dirac-Fock calculations show that the resonant Auger spectra are influenced by unusually pronounced configuration interaction in the excited state. This influence is strongly enhanced by a change of sign in the Auger amplitude of the leading term near the transition energy, a dynamic effect similar to a Cooper minimum in photoionization.

PACS number(s): 32.80.Hd, 31.20.Tz, 31.90.+s

In contrast to photoemission, Auger decay takes place at a fixed kinetic energy of the outgoing electron. Thus direct tests of the kinetic-energy dependence of the Auger amplitudes are not possible. Nevertheless, variation of the Auger emission amplitudes with excitation energy can manifest itself in experimentally observable effects. Examples are the postcollision interaction between a photoelectron and an Auger electron [1] and intensity variations in the radiationless decay of photoionization satellite states differing in the  $n$ -quantum number of an outer excited electron [2]. We found another manifestation of these dynamical variations in the investigation of resonant Auger decay of  $2p$ -photoexcited Mg. In the decays of the Mg  $2p^{-1}4s$  excited state the Auger amplitude due to the leading configuration has a sign change very near the transition energy, similar to a Cooper minimum in photoionization [3]. This induces a strongly enhanced sensitivity of these decays to configuration interaction (CI) in the intermediate state.

Theoretical [4–6] and experimental [7–11] studies of the angular anisotropy of resonant Auger decay have become feasible only recently. Resonant Auger lines are commonly classified as either participator lines, where the excited electron takes part in the decay, or spectator lines, in which it is not involved. A successful theoretical interpretation of the salient features of resonant Auger spectra has been possible within a single-configuration model for all rare gases [4,5], in particular the  $2p$  excitations of Ar, while the effects of CI have been moderately small [6]. The present experimental study of the resonant Auger decay of atomic Mg following  $2p \rightarrow 4s, 3d$  excitation and the theoretical analysis of the angular distributions of the pertinent resonant Auger lines by our multiconfiguration Dirac-Fock (MCDF) calculations are in remarkable contrast to this general trend.

In the present case the resonant Auger decay can be treated as a two-step process, since the resonantly enhanced intensity is an order of magnitude larger than the nonresonant intensity [12] and the bandpass of the photon beam is much larger than the natural lifetime of the intermediate state

excluding resonant Raman-like behavior [13]. Thus, the angular distribution of the emitted electrons after dipole excitation is given by [14]

$$W(\theta) = (W_0/4\pi) [1 + \alpha_2 \mathcal{A}_{20} P_2(\cos\theta)], \quad (1)$$

where  $W_0$  is the total decay intensity,  $\mathcal{A}_{20}$  the alignment parameter of the intermediate state, which depends on the dynamics of the resonant excitation process,  $\alpha_2$  the intrinsic anisotropy coefficient, which contains the decay matrix elements, and  $P_2$  the second-order Legendre polynomial. When photoexcitation takes place from a closed-shell atom by linearly polarized photons, then  $\mathcal{A}_{20} = -\sqrt{2}$  [8]. Hence, the experimentally observed angular anisotropy,  $\beta = \mathcal{A}_{20}\alpha_2$ , can be calculated from the decay amplitudes alone. In cases where only *one outgoing partial wave* is involved in the decay of the excited state,  $\alpha_2$  is a geometric quantity independent of the resonant decay amplitudes [8,14].

The experiment was performed at the BESSY synchrotron radiation facility in Berlin. Photons from an undulator were energy selected by a 14.9-m toroidal grating monochromator. Atomic Mg was produced in a resistively heated oven operating at approximately 500 °C. Electrons were simultaneously detected in two time-of-flight electron spectrometers mounted on a rotatable chamber, allowing for a more accurate determination of angular distributions. A more complete description of the apparatus was given previously [15]. A monochromator bandpass of about 80 meV in the region of interest was sufficient to isolate all  $2p \rightarrow 4s, 3d$  resonance excitations [12,16].

Before we examine the experimental results, it is instructive to review the expected behavior for the angular distributions of the resonant Auger lines following the decay of  $2p$ -photoexcited Mg. Mg is a closed-shell atom with ground state  $1s^2 2s^2 2p^6 3s^2 (^1S_0)$ . Unlike the rare gases, however, Mg is left with a single electron coupled to a closed Ne-like configuration following the decay of the resonantly excited  $2p$ -core-hole states. Hence, the decay spectrum consists of clearly separated lines unaffected by multiplet splitting [12]. The  $2p \rightarrow 4s$  excitations can be described in lowest order by single-configuration  $jj$ -coupled states. According to the strict-spectator model (SSM) of resonant Auger decay [4], decay of the  $2p_{3/2}^{-1}ns_{1/2}$  ( $J=1$ ) and the  $2p_{1/2}^{-1}ns_{1/2}$  ( $J=1$ )

\*Permanent address: Institute of Nuclear Physics, Moscow State University, 119 899, Moscow, Russia.

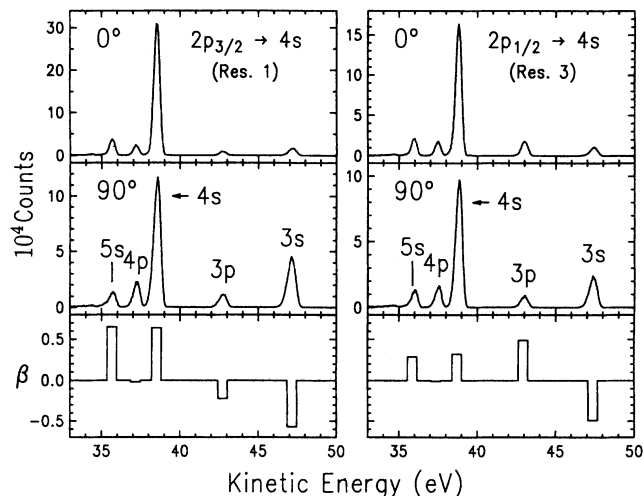


FIG. 1. Resonant Auger spectra of Mg and corresponding  $\beta$  values following  $2p_{3/2} \rightarrow 4s$  excitation, left panels, and  $2p_{1/2} \rightarrow 4s$  excitation, right panels. The spectrometer angle with respect to the electric-field vector is given in the upper left hand corner of each panel. Lines are designated according to the lone electron in the final ionic state. For a given excitation, the spectra recorded at the two different angles have been normalized with respect to each other.

excited states involves only one partial wave then. Thus, the spectator  $\beta$  values can be calculated analytically, giving  $\beta=1$  and 0, respectively.

Spectra recorded at  $\theta=0^\circ$  and  $90^\circ$  are shown in Fig. 1 for the  $2p_j \rightarrow 4s$  excitations, and in Fig. 2 for the next three resonances, which according to the absorption data [16] involve  $2p_j \rightarrow 3d$  and  $2p \rightarrow 3s3p^2$  excitations. Figures 1 and 2 show several unexpected results. The first is a marked deviation from the predictions of the SSM for the  $4s$  spectator lines in Fig. 1. For the decay of the  $2p_{3/2}^{-1}4s_{1/2}$  ( $J=1$ ) excited state we measure  $\beta=0.62(5)$ , while for  $2p_{1/2}^{-1}4s_{1/2}$  ( $J=1$ ) we find  $\beta=0.29(5)$ . The second and most striking feature is the strong negative anisotropy of the  $3s$  participator lines in Fig. 1. This is in complete contrast to the participator behavior observed in the rare gases [7] and other alkaline-earth atoms [10]. We also observe dramatic variations in the  $\beta$  value of the  $3s$  participator line of Fig. 2, which changes from a maximum value of 1.90(5) at resonance 4 to a strongly negative value of  $-0.53(5)$  at resonance 6.

In order to understand this behavior, we have performed detailed MCDF calculations. We used the MCDF code of Grant *et al.* [17] to construct all bound-state wave functions, while the continuum wave function and the transition rates were calculated using the multichannel MCDF code described in Ref. [18], neglecting, however, continuum-channel interaction. The continuum orbitals were obtained by solving the Dirac equation, including the exchange interaction, in the frozen-core field of the final ionic state. Orthogonality of bound-state orbitals of the same symmetry was enforced by Lagrange multipliers. For the calculation of the transition rates we used orbitals optimized for the intermediate state throughout. However, to partly account for relaxation, we used, for the final state, mixing coefficients between different (relativistic) configurations obtained with final-state single-particle wave functions.

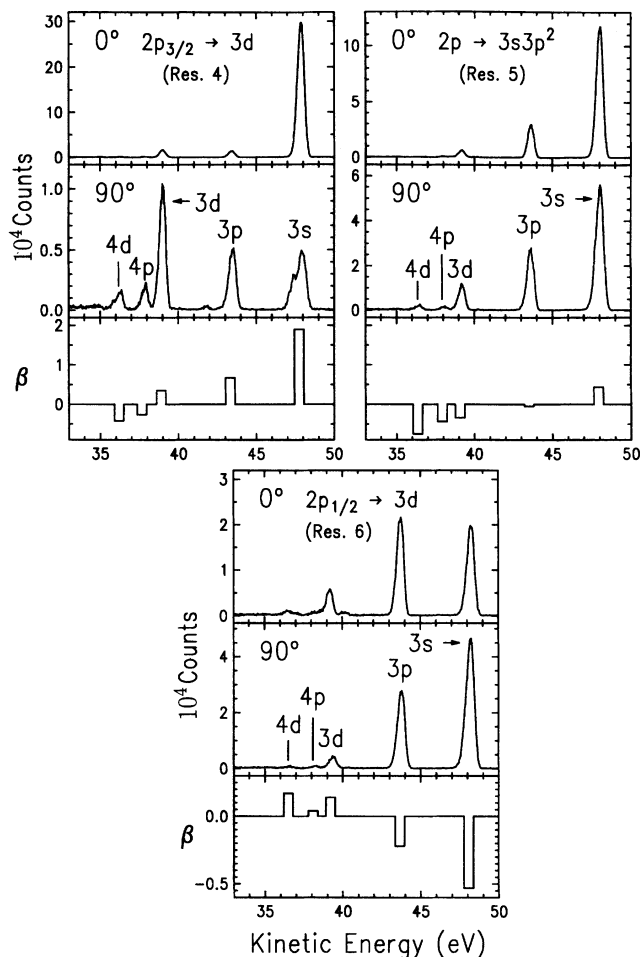


FIG. 2. Resonant Auger spectra of Mg and corresponding  $\beta$  values following  $2p_{3/2} \rightarrow 3d$  excitation, left panels,  $2p \rightarrow 3s3p^2$  excitation, right panels, and  $2p_{1/2} \rightarrow 3d$  excitation, bottom panels. All other characteristics of this figure are the same as those in Fig. 1.

While no notable CI occurs in the final state, the effect of CI in the intermediate state was decisive in the understanding of the experimental spectra. Results of the calculations are listed together with the experimental values in Table I. Each resonance is denoted by its number and designation according to Ref. [16]. To explore the effect of CI on the angular anisotropy of the resonant Auger decay, we used basis sets constructed from one (1C), two (2C), and 14 (14C) non-relativistic configurations. Each basis set consisted of all  $jj$ -coupled states with  $J=1$  that could be constructed from the nonrelativistic configurations where the following occurs.

1C consists of the  $2p^{-1}4s$  configuration for resonances 1 and 3, and a  $2p^{-1}3d$  configuration for resonances 4–6. For resonances 4 and 5 the theoretical  $\beta$  values for the two states of the  $2p_{3/2}^{-1}3d$  configuration are given, although the calculated splitting is much smaller than the energy difference between these two resonances.

2C includes in addition to 1C the  $2p^{-1}(3p^2)_{J=0}4s$  configuration for resonances 1 and 3 leading to 6 configurations in  $jj$  coupling, and a  $2p^{-1}3s3p^2$  configuration for the remaining resonances leading to 14  $jj$ -coupled configurations.

14C corresponds to a  $2p^{-1}\{3s^2ns(n=4-8)+3s^23, 4d$

TABLE I. Experimental and theoretical  $\beta$  values of the spectator and participator lines for the decay of the  $2p \rightarrow 4s, 3d$  resonances. Final-state designations refer to the lone electron outside a closed Ne core. Theoretical values are obtained using a 1C, 2C, or 14C basis set as described in the text.

Excited state	Final state	$\beta$ (exp)	$\beta$ (theory)		
			1C	2C	14C
Res. 1 $2p_{3/2}^{-1}4s$	3s	-0.57(5)	-0.11	-0.85	-0.60
	4s	0.62(5)	0.85	0.64	0.77
Res. 3 $2p_{1/2}^{-1}4s$	3s	-0.48(5)	-0.58	-0.94	-0.90
	4s	0.29(5)	0.17	0.43	0.23
Res. 4 $2p_{3/2}^{-1}3d$	3s	1.90(5)	1.80	1.92	1.98
	3d	0.32(5)	-0.23	-0.29	0.09
Res. 5 $2p^{-1}3s3p^2$	3s	0.44(5)	2.00	-0.65	0.69
	3d	-0.37(5)	-0.34	-0.36	-0.39
Res. 6 $2p_{1/2}^{-1}3d$	3s	-0.53(5)	1.98	0.51	-0.51
	3d	0.10(5)	-0.03	0.12	0.21

+  $3s3p^2 + 3s3d^2 + 3s4s^2 + (3p^2)_{J=0}4, 5s + (3p^2)_{J=0}3, 4d$  intermediate state, leading to 70  $jj$ -coupled configurations.

We note that CI between the  $2p^{-1}3s^23d$  excited configurations and the doubly excited  $2p^{-1}3s3p^2$  states is very strong. According to our 14C calculation, resonances 4–6 contain 72%, 61%, and 56%  $3d$  character, respectively.

For the  $4s$ -spectator values, Table I shows deviations from the spectator model predictions for all calculations. These deviations arise from mixing of the  $2p_{1/2}^{-1}$  and  $2p_{3/2}^{-1}$  core-hole states, permitting the emission of more than one partial wave during the decay. The calculated admixture of  $2p_{1/2}^{-1}$  to the  $2p_{3/2}^{-1}$  state and vice versa is 0.3%, 1.8%, and 0.7%. Clearly even the small mixing given by the 1C calculation reproduces the trend of the measurements, but fails to explain the results quantitatively.

Inspection of Table I indicates that the theoretical results are extremely sensitive to CI, as shown by the difference between the 2C and the 14C results. The most dramatic changes, however, occur when the configurations involving the  $3p^2$  orbitals are taken into account by the 2C calculation. The reason for these changes are twofold. The first involves a change in the wave function of the continuum electron due to orthogonalization with the now present  $3p$  electrons. This effect leads to the changes in the  $3s$   $\beta$  values at resonances 1 and 3, and the more moderate changes of the  $3d$   $\beta$  values at the other resonances. The second involves the opening of a new decay channel by which the resonant Auger lines can be populated. This effect leads to the changes in the  $4s$   $\beta$  values at resonances 1 and 3, and the  $3s$   $\beta$  values of resonances 4–6. An examination of the absolute decay rates underlines the importance of these additional decay paths. For example, at resonance 4 the  $3s$  rate is  $2.76 \mu\text{a.u.}$  and  $34.3 \mu\text{a.u.}$  for the 1C and the 2C calculations, respectively. Rate changes at the other resonances are of the same order.

To understand why CI affects both the angular anisotropy and the decay rates so strongly, we examined the behavior of the Slater integrals governing the decay dynamics. Spectator decay of the  $4s$ -excited states in the 1C calculation only

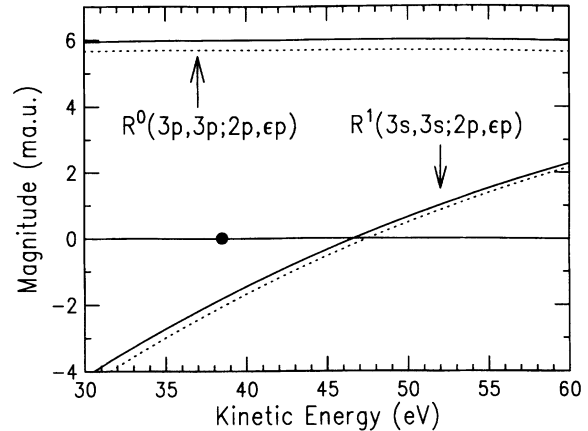


FIG. 3. Comparison of the  $R^1(3s, 3s; 2p_j, \epsilon p_j)$  Slater integrals with the  $R^0(3p_j, 3p_j; 2p_j, \epsilon p_j)$  Slater integrals as a function of the kinetic energy of the continuum electron,  $\epsilon p_j$ . Solid lines are  $j = 1/2$  and dotted lines  $j = 3/2$ . The filled circle indicates the kinetic energy of the  $4s$  spectator line following  $2p_{3/2}^{-1}4s$  excitation (see Fig. 1).

involves  $R^1(3s, 3s; 2p, \epsilon p)$  Slater integrals. However, in the 2C and 14C calculations, this decay can also involve the  $R^0(3p, 3p; 2p, \epsilon p)$  Slater integral. A plot of these integrals as a function of the kinetic energy of the continuum electron,  $\epsilon p$ , is shown in Fig. 3. The experimental kinetic energy of the  $2p_{3/2}^{-1}4s$  spectator line is indicated by the filled circle. One clearly sees that the integral involving the  $3s$  electrons changes sign very near the experimental Auger kinetic energy and is small throughout the entire kinetic-energy range shown. Thus, the contribution to the  $4s$  spectator decay from the primary  $2p^{-1}3s^24s$  configuration is suppressed by cancellation effects in the radial matrix element. This matrix element would completely vanish at a kinetic energy of 7 eV higher, in analogy to a Cooper minimum in photoionization. Hence, population of the  $4s$  spectator line is dominated not by the decay of the primary configuration but via the decay of the  $3p^24s$  configuration which is mixed in due to CI. The effect on the resonant Auger rates is further enhanced because the angular part of the transition amplitude involving the  $R^\kappa(n\ell, n\ell'; 2p, \epsilon p)$  Slater integral having rank  $\kappa=0$  is typically a factor of 5 larger than those of rank  $\kappa=1$ .

For resonances 1 and 3 this mechanism alone, which is already contained in the 2C calculation, is enough to qualitatively explain the observed anisotropy. As can be seen from Table I, however, reasonable quantitative agreement is only realized in the 14C calculation. For the participator decay of resonances 4–6, another mechanism becomes important. In the presence of the additional configurations in the 14C calculation, the  $3d$  orbital is contracted stronger. For  $3d_{5/2}(3d_{3/2})$  the mean radius  $\langle r \rangle$  changes from 9.39(9.43) a.u. to 6.30(6.15) a.u. This entails an increase of the  $R^1(3s, 3d; 2p, \epsilon p)$  Slater integrals which in turn strongly affect the participator decay. This further emphasizes the impact that CI has on the decay dynamics of this system. The remaining discrepancy in the participator line of resonance 3 could stem from the neglect of direct photoionization into the  $3s$  final state, which on a relative scale is strongest at this resonance [12]. Assuming an incoherent average between the

direct and indirect transitions to the 3s final state gives  $\beta = -0.49$ .

Although our resolution does not allow us to clearly resolve the higher members of the *nd*-Rydberg series from the *ns*-Rydberg series, our data indicate a recovery of the normal spectator behavior, as predicted by the SSM, with increasing *n*. This observation points towards a decreasing influence of CI in the higher-lying excited states.

In conclusion we have observed unexpected angular anisotropy in the resonant Auger decay of 2*p*-photoexcited Mg. Through detailed MCDF calculations using a basis set of 14 nonrelativistic configurations, we obtained reasonable agreement between theory and experiment. We have traced part of the unusually strong many-electron effects to the dynamic variation of the Auger amplitudes of the primary 4*s* excited-

state configuration and to the contraction of the excited 3*d* orbital. The dynamic variation is due to a sign change in the resonant Auger amplitude, akin to a Cooper minimum in photoionization. This phenomenon, although not previously observed, is undoubtedly not restricted to atoms alone. It also indicates the importance of properly accounting for CI, which may, as shown in this Rapid Communication completely dominate the physical behavior of a system.

This work was supported by the Bundesminister für Forschung und Technologie, the Deutsche Forschungsgemeinschaft, and the Academy of Finland. S.B.W. acknowledges support from the Alexander von Humboldt Foundation, U.H. from the Senate of Berlin, and N.M.K. from the Fritz-Haber-Institut.

- 
- [1] J. Tulkki, G. B. Armen, T. Åberg, B. Crasemann, and M. H. Chen, *Z. Phys. D* **5**, 241 (1987).
- [2] G. B. Armen and F. P. Larkins, *J. Phys. B* **24**, 741 (1991).
- [3] J. W. Cooper, *Phys. Rev.* **128**, 681 (1962).
- [4] U. Hergenhahn, B. Lohmann, N. M. Kabachnik, and U. Becker, *J. Phys. B* **26**, L117 (1993) and references therein.
- [5] M. H. Chen, *Phys. Rev. A* **47**, 3733 (1993).
- [6] J. Tulkki, H. Aksela, and N. M. Kabachnik, *Phys. Rev. A* (to be published).
- [7] T. A. Carlson, D. R. Mullins, C. E. Beall, B. W. Yates, J. W. Taylor, D. W. Lindle, and F. A. Grimm, *Phys. Rev. A* **39**, 1170 (1989).
- [8] B. Kämmerling, B. Krässig, and V. Schmidt, *J. Phys. B* **23**, 4487 (1990).
- [9] A rather complete list of experimental measurements on the rare gases can also be found in Ref. [4].
- [10] K. Ueda, J. B. West, K. J. Ross, H. Hamdy, H. J. Beyer, and H. Kleinpoppen, *Phys. Rev. A* **48**, R863 (1993); *J. Phys. B* **26**, L1 (1993).
- [11] C. D. Caldwell, S. J. Schaphorst, M. O. Krause, and J. Jiménez-Mier, *J. Elec. Spectrosc. Rel. Phenom.* **67**, 243 (1994).
- [12] S. B. Whitfield, C. D. Caldwell, and M. O. Krause, *Phys. Rev. A* **43**, 2338 (1991).
- [13] A. Kivimäki, A. Naves de Brito, S. Aksela, H. Aksela, O.-P. Sairanen, A. Ausmees, S. Osborne, L. B. Dantas, and S. Svensson, *Phys. Rev. Lett.* **71**, 4307 (1993).
- [14] N. M. Kabachnik and I. P. Sazhina, *J. Phys. B* **17**, 1335 (1984).
- [15] U. Becker, D. Szostak, H. G. Kerkhoff, M. Kupsch, B. Langer, R. Wehlitz, A. Yagishita, and T. A. Hayaishi, *Phys. Rev. A* **39**, 3902 (1989).
- [16] D. L. Ederer, T. B. Lucatorto, and G. Mehlman, *J. Opt. Soc. Am.* **69**, 520 (1979) and references therein.
- [17] I. P. Grant, B. J. McKenzie, P. H. Norrington, D. F. Mayers, and N. C. Pyper, *Comput. Phys. Commun.* **21**, 207 (1980).
- [18] J. Tulkki, T. Åberg, A. Mäntykenttä, and H. Aksela, *Phys. Rev. A* **46**, 1357 (1992).